Cancer Imaging (2009) **9,** S115–S121
DOI: 10.1102/1470-7330.2009.9043

CI

e-med
www.e-med.org.uk

The child with bone pain: malignancies and mimickers

M. Beth McCarville

Department of Radiological Sciences, Division of Diagnostic Imaging, St. Jude Children's Research Hospital, Memphis, TN 38105, USA

Corresponding address: M. Beth McCarville, MD, Department of Radiological Sciences, St. Jude Children's Research Hospital, 262 Danny Thomas Place, Mail Stop 210, Memphis, TN 38105, USA.
Email: beth.mccarville@stjude.org

Abstract

Bone pain in children is common. The cause may be as benign as growing pains or as life-threatening as a malignancy. When a cause cannot be established by laboratory tests, physical examination or patient history, imaging of the affected body part is often obtained. Distinguishing benign from malignant processes involving the bones of children, based on imaging findings, can be challenging. The most common benign conditions that mimic pediatric bone tumors on imaging are Langerhan's cell histiocytosis and osteomyelitis. In this review, the current literature regarding the pathology and imaging of these conditions is reviewed. Benign conditions are compared with the most common pediatric bone tumors, Ewing sarcoma and osteosarcoma, with an emphasis on clinical and imaging features that may aid in diagnosis.

Keywords: *Langerhan's cell histiocytosis; osteomyelitis; Ewing sarcoma; osteosarcoma.*

Introduction

Bone pain in children is common. The cause may be as benign as growing pains or as life-threatening as a malignancy. When a cause cannot be established by laboratory tests, physical examination or patient history, imaging of the affected body part is often obtained. Distinguishing benign from malignant processes involving the bones of children, based on imaging findings, can be challenging. The most common benign conditions that mimic pediatric bone tumors on imaging are Langerhan's cell histiocytosis and osteomyelitis. In this review, the current literature regarding the pathology and imaging of these conditions is reviewed. Benign conditions are compared with the most common pediatric bone tumors, Ewing sarcoma and osteosarcoma, with an emphasis on clinical and imaging features that may aid in diagnosis.

Langerhan's cell histiocytosis

The histopathology of Langerhan's cell histiocytosis (LCH) is that of a granulomatous lesion containing pathologic Langerhan's cells, normal inflammatory cells and multinucleated giant cells. The peak incidence of LCH is between 1 and 4 years of age, however, it can present at any age, from newborn to adulthood, in three different forms. At one end of the spectrum are patients with single-system disease (eosinophilic granuloma; EG) who have 100% survival with minimal or no therapy. At the other end are patients, usually young children, with disseminated life-threatening disease (Letterer–Siwe disease) that can involve any organ. In between are patients whose disease runs a chronic, fluctuating course (Hand–Shüller–Christian disease) that eventually burns out but frequently leaves serious residual disabilities. Bone is the commonest single organ to be involved in childhood LCH and most patients present with a solitary lesion and an excellent outcome. The most common presentation is a single mass lesion on the skull, although all bones may be involved (Fig. 1A). Patients with bone involvement present with swelling and/or pain that is initially only present at night. LCH is the commonest cause of vertebra plana in children, and when there is an associated soft tissue mass, can cause neurological symptoms[1–4].

The imaging evaluation of LCH should begin with a complete skeletal survey. The role of nuclear technetium-99m (^{99m}Tc) bone scintigraphy is somewhat controversial because up to 20% of bone lesions may be missed by this modality. ^{18}F-labeled fluorodeoxyglucose (FDG)

1470-7330/09/000115 + 07

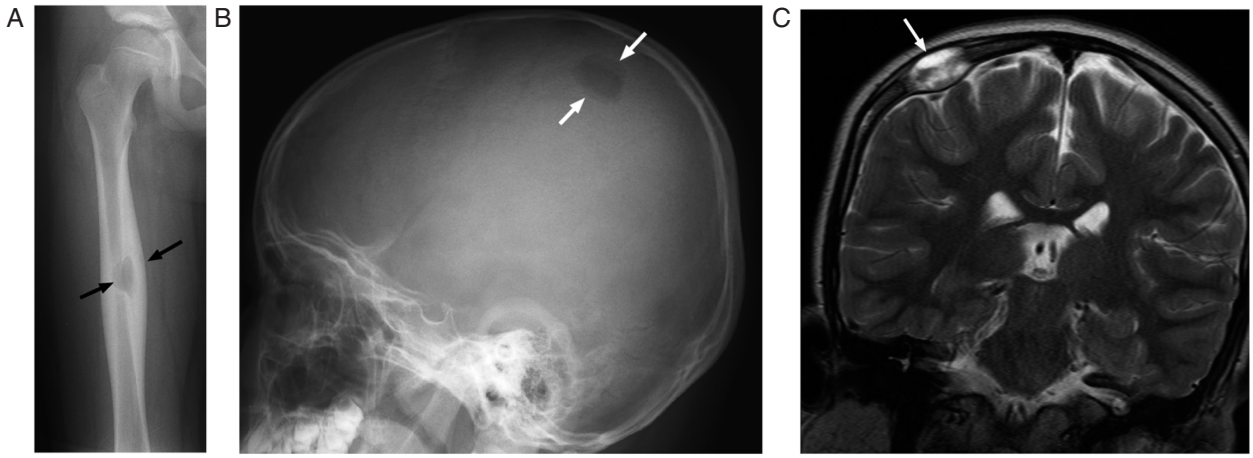

Figure 1 **An 8-year-old girl with Langerhan's cell histiocytosis (LCH) presented with right thigh pain. (A) This anterior-posterior (AP) radiograph shows a lytic lesion surrounded by cortical thickening (arrows) in the diaphysis of the right femur. The femur is a common site of involvement in LCH. (B) The patient also had a skull lesion as shown in this lateral skull x-ray (arrows). Note the beveled edges of this lesion, a feature typical of LCH. (C) This coronal T2-weighted MRI shows the soft tissue component (arrows) of the skull lesion. The skull is the most common site of bone disease in LCH and patients often present with a palpable scalp mass.**

positron emission tomography (PET) imaging is emerging as a valuable tool in LCH because it reflects intralesional metabolic activity and, therefore, may be more sensitive than skeletal survey and ^{99m}Tc bone scan for the detection of active lesions and more useful as an indicator of disease response to therapy. Computed tomography is useful for further characterization of lesions involving the flat bones, such as the skull base, pelvis and scapula, which can be difficult to visualize on plain films. Magnetic resonance imaging (MRI) is useful in evaluating lesions of the long bones, skull and central nervous system (Fig. 1B). There has been recent interest in whole-body MRI to demonstrate osseous, soft tissue and nodal involvement, without the use of radiation[5–9].

LCH has a predilection for flat bones, however, one-third of lesions occur in long bones, most commonly the femur (Fig. 1C). The radiographic appearance depends on the phase of disease. In the acute phase, on radiography, LCH frequently has an aggressive, permeative and lytic appearance, with poorly defined margins, similar to that seen in Ewing sarcoma and osteomyelitis. The lesions may be expansile, especially those arising in the ribs, scapula and clavicles. Lytic lesions of LCH may contain a fragment of intact bone, known as a sequestrum, that can be helpful in distinguishing them from a malignancy. As lesions regress, they become better defined and eventually are surrounded by reactive sclerosis. MRI can depict the bone marrow involvement and associated soft tissue mass, when present. The lytic component seen on radiography will appear hypointense on T1-weighted (T1W) images and hyperintense on T2-weighted (T2W) and short tau inversion (STIR) images. In the acute phase there is often edema of adjacent marrow and soft tissues which intensely enhances with gadolinium. As lesions heal they show a decrease in T2W and STIR signal intensity[5–8]. The imaging findings of LCH are non-specific and can appear similar to Ewing sarcoma, bone metastases and osteomyelitis. The diagnosis is clinicopathologic and is based on clinical findings and histologic/immunohistochemical criteria. The presence of racquet-shaped, Birbeck granules by CD1a immunohistochemistry or electron microscopy is confirmatory[1–4].

Osteomyelitis

Most cases of osteomyelitis in children arise hematogenously and commonly affect the metaphyses of long bones, especially the distal femur and proximal tibia; sites also commonly involved by osteosarcoma. The clinical presentation of children can be elusive. Toddlers may present with limping or pain on passive movement. A preceding history of trauma is common but the role of trauma in the pathogenesis of osteomyelitis in children is unclear. Clinical and laboratory findings, including fever, elevated erythrocyte rate or C-reactive protein and leukocytosis, are non-specific and these factors can even be normal. Serial blood cultures are positive in only 32–60% of cases[10]. Culture of material aspirated from the affected bone can be negative in 40–60% of cases[11]. The most common organism is *Staphylococcus aureus*, followed by β-hemolytic streptococcus, *Streptococcus pneumoniae*, *Escheria coli* and *Pseudominas aeruginosa*[10].

Osteomyelitis is frequently designated as acute, subacute and chronic and may involve a single bone or multiple bones. Acute osteomyelitis is a suppurative infection accompanied by edema, vascular congestion and small vessel thrombosis. As the infection spreads through the

medullary canal, increasing pressure causes extension to the cortex through Havers and Volkmann's canals with subsequent spread to the subperiosteal space and, if untreated, to the periosteum and adjacent soft tissue. When both the medullary and periosteal blood supplies are compromised, large sequestra, similar to those seen in LCH, may form. Sequestra can reside in marrow for extended periods of time, harboring viable organisms than can evoke a flare-up of infection. An involucrum denotes a layer of living bone that forms around dead bone. The involucrum often is perforated by openings (cloaca) through which pus may track into surrounding soft tissue and eventually to the skin surface. Co-existence of infected, non-viable tissue and an ineffective host response leads to disease chronicity[10].

Plain film findings of osteomyelitis lag the onset of infection by days to weeks. Initial findings may include only subtle soft tissue edema near the involved metaphysis. Radiographically evident bone destruction and periosteal reaction take 2–3 weeks to develop. Eventually metaphyseal lucencies with varying degrees of cortical destruction and periosteal new bone develop. The periosteal reaction can appear as lamellated, onion-skin or spiculated new bone or a Codman's triangle due to subperiosteal abscess. After 10–12 weeks, regenerative changes occur with a sclerotic response (Fig. 2A)[10].

MRI is more sensitive to the early changes of osteomyelitis because of the excellent contrast between normal and abnormal marrow as well as depiction of surrounding soft tissue changes. In the acute phase the marrow edema will have low signal intensity of T1W images and high signal intensity of T2W and STIR images. The adjacent cortex may be disrupted and can have abnormal signal intensity. Gadolinium may define areas of necrosis and is useful in demonstrating bone and soft tissue abscess on T1W images. MRI can demonstrate the characteristic tracts from bone marrow, through cortex into soft tissue, which can distinguish osteomyelitis from tumor (Fig. 2A,B). Subperiosteal fluid collections are also a useful sign in distinguishing infection from malignancy[10–13].

In subacute and chronic osteomyelitis a Brodie's abscess can develop. These occur in the metaphyses and can range from 1 to 4 cm in diameter. The wall of the abscess is lined by granulation tissue and the fluid is composed of pus or mucoid material. On plain radiography these appear as a rounded lucency with surrounding sclerosis. On MRI the central cavity will appear as low signal intensity on T1W images and bright signal intensity on T2W and STIR images. The rim of sclerotic bone will be dark on all sequences. A rim of peripheral enhancement is often seen after administration of gadolinium. In the chronic phase of osteomyelitis the marrow becomes fibrotic resulting in low signal intensity on T2W and STIR imaging. Cortical thickening is apparent on plain radiography and MRI. The transition zone with normal marrow becomes narrower and sharply defined in the chronic phase in contrast to a wide zone of transition seen in the acute phase[10–13].

Ewing sarcoma

The Ewing sarcoma family of tumors includes Ewing sarcoma of bone, extraskeletal Ewing sarcoma, Askin tumor of the thoracic wall and peripheral primitive neuroectodermal tumor. These small blue round cell tumors are highly aggressive, poorly differentiated malignancies of unknown histogenesis. Ewing sarcoma (EWS) is the second most common primary bone malignancy in childhood, after osteosarcoma. The peak incidence is 15 years of age although it can be seen into the fourth decade. Patients present with local-regional pain, that may be intermittent and less severe at night. Pain without a history of trauma, lasting longer than a month or persisting at night should prompt imaging evaluation[14].

The initial imaging evaluation is generally plain radiography which is extremely useful in patients with malignant bone tumors and usually suggests the malignant nature of the lesion. EWS most often affects the long bones of the lower extremity followed by the pelvis and spine. In the long bones it affects the metadiaphysis or the diaphysis. On plain radiography, the appearance is variable. Most often EWS appears as a poorly marginated, intramedullary lytic lesion. It may have a permeative appearance or appear as a mixed lytic and sclerotic lesion or be predominantly sclerotic. The lesions are usually associated with an aggressive lamellated or spiculated periosteal reaction, with or without a large soft tissue mass (Fig. 3A–C)[15,16].

MRI is the preferred imaging modality for assessing EWS because it provides excellent tissue contrast and can assess tumor extent, size and relationship to the neurovascular bundle and joint space. On MRI these tumors will appear heterogenous but predominantly have low signal intensity on T1W images and increased signal intensity on T2W and STIR images. The tumors show variable contrast enhancement due to areas of necrosis. It can be difficult to distinguish tumor margins due to the presence of peritumoral edema on MRI (Fig. 3B)[15–18].

Osteosarcoma

Osteosarcoma is the most common primary malignant bone tumor of childhood. It arises from primitive bone-forming mesenchyme and is characterized by the production of osteoid or immature bone by the malignant proliferating spindle cell stroma. The peak incidence is in the second decade of life during the adolescent growth spurt. It is felt that there is a causal relationship between the rapid bone growth seen during adolescence and the development of this malignancy. This relationship also explains the predilection of this tumor to involve the metaphyses of the most rapidly growing bones during

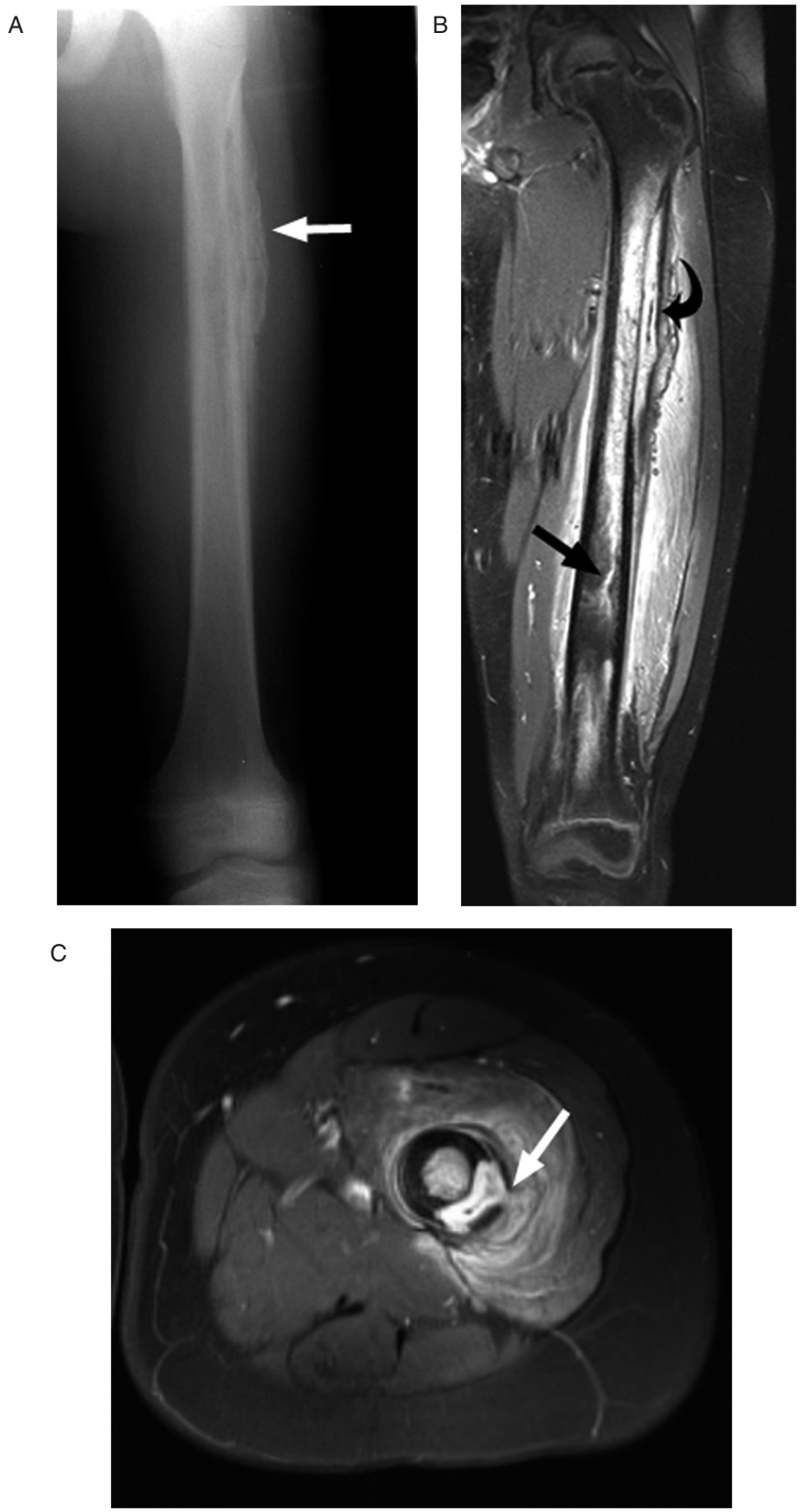

Figure 2 **A 12-year-old boy with a 2-month history of limp and leg pain following minor trauma was found by biopsy to have chronic osteomyelitis. The patient was afebrile and had a normal white blood cell count but elevated C-reactive protein at the time of imaging. (A) This AP radiograph shows coarse, thickened periosteum (arrow). (B) This gadolinium-enhanced coronal MR image shows a subperiosteal abscess (curved arrow) and enhancing tract extending into the distal metadiaphysis. (C) This axial gadolinium-enhanced image shows a tract extending from the subperiosteal abscess into the abnormally enhancing surrounding muscle (arrow).**

Figure 3 **A 10-year-old girl with a 1-year history of right leg pain due to Ewing sarcoma. (A) This AP radiograph shows thick lamellated, periosteal reaction in the mid-shaft of the right femur (arrows). (B) This short tau inversion recovery (STIR) coronal MR image shows the poorly defined tumor infiltrating the marrow space (straight arrows) and thick periosteal reaction surrounded by soft tissue edema (curved arrows). (C) This axial contrast-enhanced MR image shows the enhancing marrow tumor (straight arrow) and thick, lamellated, periosteal reaction (curved arrow). The mid-shaft location and lamellated periosteal reaction are features typical of Ewing sarcoma.**

Figure 4 **A 15-year-old girl with a 2-month history of left leg pain found to have osteosarcoma. (A) This AP radiograph shows the poorly marginated, predominantly sclerotic osteosarcoma with exuberant sunburst periosteal reaction. (B) This coronal gadolinium-enhanced MR image shows the intramedullary extent of the tumor. Non-enhancing areas in the medullary canal correspond to ossified and sclerotic components of this bone-forming tumor. Note the sharp distal tumor margin (arrow) sometimes seen in osteosarcoma. (C) This axial gadolinium-enhanced MR image shows the sunburst periosteal reaction surrounding the sclerotic marrow tumor.**

this period: the distal femur, proximal tibia and proximal humerus. Most patients with osteosarcoma present with pain over the affected area, with or without an associated soft tissue mass. The average duration of symptoms is 3 months, but it is not unusual for patients to have a history of pain for 6 months or longer[19].

Plain radiographs of conventional, intramedullary osteosarcoma most commonly show a mixed lytic and sclerotic lesion causing cortical destruction, often with an associated soft tissue mass that may contain calcification. Various periosteal reactions may be present but the most common is the sunburst, spiculated type (Fig. 4A–C). This feature is nearly pathognomonic of osteosarcoma but can also be seen with osteoblastic metastasis. A Codman's triangle is common in osteosarcoma, but is less specific and is seen in other neoplastic and non-neoplastic processes including EWS and osteomyelitis[19,20].

Similar to EWS, on MRI these tumors show low signal intensity on T1W images and high signal intensity on T2W and STIR images. Not surprisingly, the more densely calcified tumors show more low signal areas on all sequences. The tumor may have sharply defined margins on MRI or poorly defined margins inseparable from surrounding edema (Fig. 4B)[17,18,20]. MRI is extremely valuable in determining transphyseal spread of tumor into the epiphysis and involvement of the neurovascular bundle, features that impact surgical management.

Conclusions

In conclusion, bone pain in children is common and can be due to benign or malignant processes. In addition to those reviewed here, stress fracture and osteoid osteoma are benign conditions that commonly occur during childhood and can sometimes cause diagnostic dilemmas. Metastatic bone disease from neuroblastoma, leukemia and lymphoma should be considered in the appropriate clinical setting. Imaging is valuable in assessing children with bone pain but should be interpreted in conjunction with clinical features including the patient's age, laboratory findings and presenting symptoms.

References

[1] Weitzman S, Egeler RM. Langerhans cell histiocytosis: update for the pediatrician. Curr Opin Pediatr 2008; 20: 23–9. doi:10.1097/MOP.0b013e3282f45ba4. PMid:18197035.

[2] Arkader A, Glotzbecker M, Hosalkar HS, Dormans JP. Primary musculoskeletal Langerhans cell histiocytosis in children: an analysis for a 3-decade period. J Pediatr Orthop 2009; 29: 201–7.

[3] Yagci B, Varan A, Caglar M, *et al.* Langerhans cell histiocytosis: retrospective analysis of 217 cases in a single center. Pediatr Hematol Oncol 2008; 25: 399–408. doi:10.1080/08880010802107356. PMid:18569842.

[4] Egeler RM, D'Angio GJ. Langerhans cell histiocytosis. J Pediatr 1995; 127: 1–11.

[5] Herman TE, Siegel MJ. Langerhans cell histiocytosis: radiographic images in pediatrics. Clin Pediatr (Phila) 2009; 48: 228–31.

[6] Azouz EM, Saigal G, Rodriguez MM, Podda A. Langerhans' cell histiocytosis: pathology, imaging and treatment of skeletal involvement. Pediatr Radiol 2005; 35: 103–15. doi:10.1007/s00247-004-1262-0. PMid:15289942.

[7] Hoover KB, Rosenthal DI, Mankin H. Langerhans cell histiocytosis. Skeletal Radiol 2007; 36: 95–104. doi:10.1007/s00256-006-0193-2. PMid:17028900.

[8] Goo HW, Yang DH, Ra YS, *et al.* Whole-body MRI of Langerhans cell histiocytosis: comparison with radiography and bone scintigraphy. Pediatr Radiol 2006; 36: 1019–31. doi:10.1007/s00247-006-0246-7. PMid:16896695.

[9] Kaste SC, Rodriguez-Galindo C, McCarville ME, Shulkin BL. PET-CT in pediatric Langerhans cell histiocytosis. Pediatr Radiol 2007; 37: 615–22. doi:10.1007/s00247-007-0467-4. PMid:17564738.

[10] Pineda C, Vargas A, Rodriguez AV. Imaging of osteomyelitis: current concepts. Infect Dis Clin North Am 2006; 20: 789–825. doi:10.1016/j.idc.2006.09.009. PMid:17118291.

[11] Wu JS, Gorbachova T, Morrison WB, Haims AH. Imaging-guided bone biopsy for osteomyelitis: are there factors associated with positive or negative cultures? AJR Am J Roentgenol 2007; 188: 1529–34. doi:10.2214/AJR.06.1286. PMid:17515372.

[12] Erdman WA, Tamburro F, Jayson HT, Weatherall PT, Ferry KB, Peshock RM. Osteomyelitis: characteristics and pitfalls of diagnosis with MR imaging. Radiology 1991; 180: 533–9.

[13] Averill LW, Hernandez A, Gonzalez L, Pena AH, Jaramillo D. Diagnosis of osteomyelitis in children: utility of fat-suppressed contrast-enhanced MRI. AJR Am J Roentgenol 2009; 192: 1232–8. doi:10.2214/AJR.07.3400. PMid:19380545.

[14] Bernstein M, Kovar H, Paulussen M. *et al.* Ewing sarcoma family of tumors: Ewing sarcoma of bone and soft tissue and the peripheral primitive neuroectodermal tumors. In: Pizzo PA, Poplack DG, editors. Principles and practice of pediatric oncology. 5th ed. Lippincott Williams & Wilkins; 2006, p. 1002–32.

[15] Mar WA, Taljanovic MS, Bagatell R, *et al.* Update on imaging and treatment of Ewing sarcoma family tumors: what the radiologist needs to know. J Comput Assist Tomogr 2008; 32: 108–18. doi:10.1097/RCT.0b013e31805c030f. PMid:18303298.

[16] Meyer JS, Nadel HR, Marina N, *et al.* Imaging guidelines for children with Ewing sarcoma and osteosarcoma: a report from the Children's Oncology Group Bone Tumor Committee. Pediatr Blood Cancer 2008; 51: 163–70. doi:10.1002/pbc.21596.

[17] Meyer JS, Dormans JP. Differential diagnosis of pediatric musculoskeletal masses. Magn Reson Imaging Clin N Am 1998; 6: 561–77.

[18] James SL, Panicek DM, Davies AM. Bone marrow oedema associated with benign and malignant bone tumours. Eur J Radiol 2008; 67: 11–21. doi:10.1016/j.ejrad.2008.01.052. PMid:18358660.

[19] Link MP, Gebhardt MC, Meyers PA. Osteosarcoma. In: Pizzo PA, Poplack DG, editors. Principles and practice of pediatric oncology. 5th ed. Lippincott Williams & Wilkins; 2006, p. 1075–115.

[20] Suresh S, Saifuddin A. Radiological appearances of appendicular osteosarcoma: a comprehensive pictorial review. Clin Radiol 2007; 62: 314–23. doi:10.1016/j.crad.2006.11.002. PMid:17331824.